

AD-A042 282

AEROSPACE CORP EL SEGUNDO CALIF AEROPHYSICS LAB  
AN ANNULAR IODINE LASER FACILITY.(U)

F/G 20/5

UNCLASSIFIED

JUN 77 E B TURNER, R A CHODZKO, R W GROSS

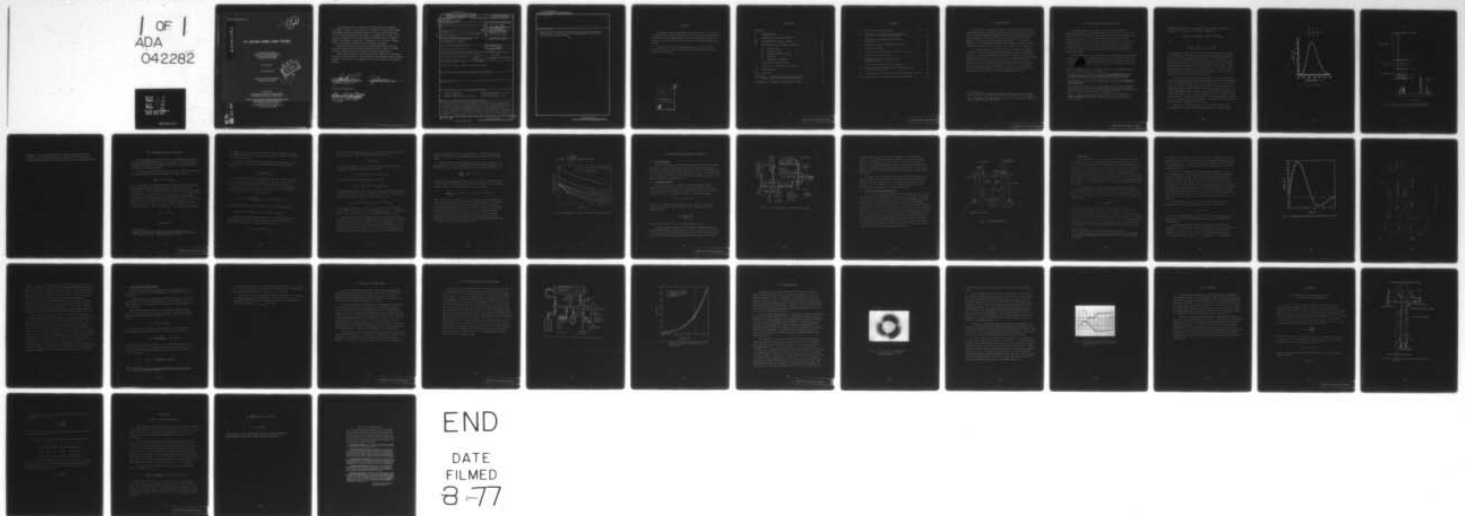
F04701-76-C-0077

TR-0077(2605)-2

SAMSO-TR-77-108

NL

1 OF 1  
ADA  
042282



AD A 042 282

2 (12)

## An Annular Iodine Laser Facility

Aerophysics Laboratory  
The Ivan A. Getting Laboratories  
The Aerospace Corporation  
El Segundo, Calif. 90245

15 June 1977

Interim Report

APPROVED FOR PUBLIC RELEASE:  
DISTRIBUTION UNLIMITED



Prepared for  
AIR FORCE WEAPONS LABORATORY  
Kirtland Air Force Base, N. Mex. 87117


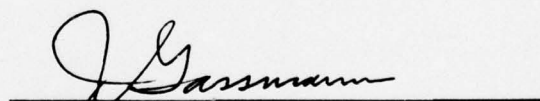
SPACE AND MISSILE SYSTEMS ORGANIZATION  
AIR FORCE SYSTEMS COMMAND  
Los Angeles Air Force Station  
P.O. Box 92960, Worldway Postal Center  
Los Angeles, Calif. 90009

AD No. \_\_\_\_\_  
DDC FILE COPY


This interim report was submitted by The Aerospace Corporation, El Segundo, CA 90245, under Contract No. F04701-76-C-0077 with the Space and Missile Systems Organization, Deputy for Advanced Space Programs, P.O. Box 92960, Worldway Postal Center, Los Angeles, CA 90009. It was reviewed and approved for The Aerospace Corporation by W. R. Warren, Director, Aerophysics Laboratory. Lieutenant A. G. Fernandez, SAMSO/YAPT, was the project officer for Advanced Space Programs.

This report has been reviewed by the Information Office (OI) and is releasable to the National Technical Information Service (NTIS). At NTIS, it will be available to the general public, including foreign nations.

This technical report has been reviewed and is approved for publication. Publication of this report does not constitute Air Force Approval of the report's findings or conclusions. It is published only for the exchange and stimulation of ideas.

  
Arturo G. Fernandez, Lt, USAF  
Project Officer  
Joseph Gassmann, Maj, USAF

FOR THE COMMANDER

  
Leonard E. Baltzer, Col, USAF  
Asst. Deputy, Advanced Space  
Programs

UNCLASSIFIED

SECURITY CLASSIFICATION OF THIS PAGE (When Data Entered)

19 REPORT DOCUMENTATION PAGE		READ INSTRUCTIONS BEFORE COMPLETING FORM
1. REPORT NUMBER (18) SAMSO-TR-77-108	2. GOVT ACCESSION NO.	3. RECIPIENT'S CATALOG NUMBER
4. TITLE (and Subtitle) (6) AN ANNULAR IODINE LASER FACILITY.	5. TYPE OF REPORT & PERIOD COVERED (9) Interim <i>1 rept.</i>	6. PERFORMING ORG. REPORT NUMBER (14) TR-0077(2605)-2
7. AUTHOR(s) (10) Eugene B. Turner, Richard A. Chodzko and Rolf W. F. Gross	8. CONTRACT OR GRANT NUMBER(s) (15) F04701-76-C-0077	
9. PERFORMING ORGANIZATION NAME AND ADDRESS The Aerospace Corporation El Segundo, Calif. 90245	10. PROGRAM ELEMENT, PROJECT, TASK AREA & WORK UNIT NUMBERS	
11. CONTROLLING OFFICE NAME AND ADDRESS Air Force Weapons Laboratory Kirtland Air Force Base, N. Mex. 87117	12. REPORT DATE (11) 15 June 1977	13. NUMBER OF PAGES 44
14. MONITORING AGENCY NAME & ADDRESS (if different from Controlling Office) Space and Missiles Systems Organization Air Force Systems Command Los Angeles, Calif. 90009 (12) 44p.	15. SECURITY CLASS. (of this report) Unclassified	15a. DECLASSIFICATION/DOWNGRADING SCHEDULE
16. DISTRIBUTION STATEMENT (of this Report)  Approved for public release; distribution unlimited		
17. DISTRIBUTION STATEMENT (of the abstract entered in Block 20, if different from Report)		
18. SUPPLEMENTARY NOTES		
19. KEY WORDS (Continue on reverse side if necessary and identify by block number)  Atomic Iodine Laser                      Flashlamp Photolysis Pumping Annular Configuration                  Engineering Design Annular Unstable-Cavity Resonators    Perfluoroalkyl Iodide Vapor		
20. ABSTRACT (Continue on reverse side if necessary and identify by block number)  The design and performance of an annular iodine laser built to study annular resonators at a large Fresnel number are described. A high-intensity axial flashlamp is used to dissociate $C_3F_7I$ vapor in the annular lasing region. The excited iodine atoms resulting from this dissociation produce radiation of 1.315 $\mu m$ wavelength by stimulated transition to the ground state. The pulsed energy output of 12.5 J was close to the performance estimates, which also indicated a small signal gain of 6.2 per meter, required for saturation of the		

DD FORM 1473  
(FACSIMILE)

409367

UNCLASSIFIED  
SECURITY CLASSIFICATION OF THIS PAGE (When Data Entered)



UNCLASSIFIED

SECURITY CLASSIFICATION OF THIS PAGE(When Data Entered)

19. KEY WORDS (Continued)

20. ABSTRACT (Continued)

medium, could be obtained. The details of the high-voltage capacitor discharge circuit, the vacuum and gas handling system, and the laser tube fabrication are described.

UNCLASSIFIED

SECURITY CLASSIFICATION OF THIS PAGE(When Data Entered)

## PREFACE

The authors wish to acknowledge the dedicated work of S. B. Mason, who fabricated the fused-quartz annular laser tube and gas-handling system, assembled the high-voltage electrical system and laser-tube mounts, set up the optical resonator and auxiliary optical system, and operated the laser system.

The authors also wish to acknowledge the work of E. F. Cross, J. A. McKay, and J. M. Narduzzi in obtaining the infrared vidicon pictures of the laser output.

ACCESSION FOR	
NTIS	Write Section <input checked="checked" type="checkbox"/>
DIC	Buff Section <input type="checkbox"/>
UNANNOUNCED	<input type="checkbox"/>
JUSTIFICATION.....	
BY.....	
DISTRIBUTION/AVAILABILITY CODES	
Dist.	Avail. Gen. or Special
A	

## CONTENTS

PREFACE .....	1
I. REQUIREMENTS .....	7
II. IODINE-LASER CHARACTERISTICS .....	9
III. PERFORMANCE CALCULATIONS .....	15
IV. HIGH-VOLTAGE ELECTRICAL CIRCUITS .....	21
A. System Design .....	21
B. Charging Circuit .....	21
C. Capacitor and Spark Switch .....	23
D. Flashlamp .....	25
E. Inductance Calculations .....	30
V. LASER-TUBE FABRICATIONS .....	33
VI. VACUUM AND GAS-HANDLING SYSTEM .....	35
VII. PERFORMANCE .....	39
VIII. SUMMARY .....	43
APPENDIX A. THRESHOLD GAIN OF CONVERGING- WAVE, UNSTABLE-CAVITY RESONATOR .....	45
APPENDIX B. CURRENT MEASUREMENT PROBE .....	49

## FIGURES

1.	Ultraviolet Absorption of $C_3F_7I$ . . . . .	11
2.	Energy Levels of Excited and Ground States of Atomic Iodine and Allowed Transitions. . . . .	12
3.	Distribution of Radiation Flux in Annular Lasing Zone . . . . .	19
4.	Schematic Diagram of High-Voltage Circuits . . . . .	22
5.	High-Voltage Switch . . . . .	24
6.	Theoretical Flashlamp Current Pulse for $V_c = 50$ kV . . . . .	27
7.	Cross Section of Iodine Laser. . . . .	28
8.	Schematic Diagram of Vacuum and Gas-Handling System. . . . .	36
9.	$C_3F_7I$ Vapor Pressure Versus Temperature . . . . .	37
10.	Near-Field Intensity Distribution of Iodine Laser with Fabry-Perot Resonator . . . . .	40
11.	Oscilloscope Traces of Laser Output and Flashlamp Current. . . . .	42
A-1.	Converging-Wave Cavity Schematic Optical Diagram . . . . .	46



## I. REQUIREMENTS

This iodine laser facility was designed and fabricated to provide an unobstructed annular gain medium for testing the converging-wave, unstable laser resonator developed by Chodsko<sup>1</sup> at a relatively high Fresnel number. Other annular laser resonators can also be tested with this iodine laser facility. Because of the relatively short wavelength ( $\lambda = 1.315 \mu\text{m}$ ) of an iodine laser, it was possible to obtain a medium Fresnel number\* ( $N_m$ ) of 1900 with an annular laser tube of 10-cm outer diameter and a length of 1 m.

A relatively high gain is required for the converging-wave unstable resonator. Calculations for the threshold gain over the range of expected values of the resonator magnification are given in Appendix A. The small signal gain ( $g_0 L$ ) should be at least ten times the maximum expected threshold gain to ensure that the medium is well saturated. This derived small signal gain of 6.5 probably can be achieved (Section III). The gain can be reduced, if desired, by the introduction of a buffer gas such as argon to increase the line broadening. The annular configuration is ideal for flash-photolysis pumping by a linear flashlamp located at the tube axis.

---

\*The Fresnel number of the medium ( $N_m$ ) is  $a^2/\lambda L$ , where  $a$  is the radius of the laser tube,  $L$  the length, and  $\lambda$  the wavelength of the laser radiation.

<sup>1</sup>R. A. Chodsko, S. B. Mason, and E. F. Cross, "Annular Converging Wave Cavity," Appl. Opt. 15, 2137 (1976).

## II. IODINE-LASER CHARACTERISTICS

The atomic iodine laser, which operates by the photochemical dissociation of certain perfluoroalkyl iodides, was discovered by Kasper and Pimentel<sup>2</sup> in 1964. Research and development of the atomic iodine laser has been increasing since 1970 when Hola and Kompa<sup>3</sup> and others realized that this type of laser is well suited for laser fusion experiments. Hola and Kompa,<sup>4</sup> Davis et al.,<sup>5</sup> and Gross<sup>6</sup> reviewed the theory and operation of the photochemical iodine laser. Their reviews contain extensive lists of references. Only a brief description of the principles of operation will be given in this report.

The pumping of the excited iodine atoms is accomplished by the photodissociation of a gaseous perfluoroalkyl iodide such as  $C_3F_7I$ . More than 90% of the iodine atoms, separated from the molecule by absorption of ultraviolet radiation, are in the excited state ( $^2P_{1/2}$ ). These excited iodine atoms then

---

<sup>2</sup>J. V. V. Kasper and G. C. Pimentel, "Atomic Iodine Photodissociation Laser," *Appl. Phys. Lett.* **5**, 231 (1964).

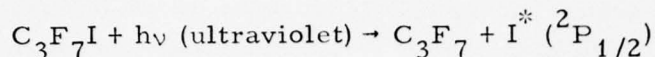
<sup>3</sup>K. Hohla, P. Gensel, and K. L. Kompa, in *Proceedings of the Second Workshop on Laser Interaction and Related Plasma Phenomena*, eds., J. Schwarz and H. Hora, Plenum Publishing Co., New York (1972).

<sup>4</sup>K. Hola and K. L. Kompa, "The Photochemical Iodine Laser," *Chemical Laser Handbook*, eds., R. W. F. Gross and J. F. Bott, Wiley-Interscience, New York (1976).

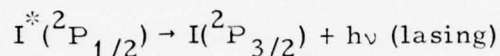
<sup>5</sup>C. C. Davis, R. J. Pirkle, R. A. McFarlane, and G. J. Wolga, "Output Mode Spectra, Comparative Parametric Operation, Quenching, Photolytic Reversibility, and Short-Pulse Generation in Atomic Iodine Photodissociation Lasers," *IEEE J. Quantum Electron.* **QE-12**, 334 (1976).

<sup>6</sup>R. F. W. Gross, "Laser Induced Fusion and X-Ray Laser Studies," in *Physics of Quantum Electronics*, Vol. III, eds., S. F. Jacobs, M. O. Scully, M. Sargent, and C. D. Cantrell III, Addison-Wesley, Reading, Mass. (1976).

make the transition to the ground state ( $^2P_{3/2}$ ), with the emission of radiation at  $\lambda = 1.315 \mu\text{m}$ . The primary reactions are:



and



The absorption band of  $\text{C}_3\text{F}_7\text{I}$  (Fig. 1) extends from about 0.24 to 0.32  $\mu\text{m}$  in the ultraviolet. Such iodide molecules as  $\text{CF}_3\text{I}$ ,  $\text{C}_2\text{F}_5\text{I}$ , and  $\text{C}_4\text{F}_9\text{I}$  have also been used for photochemical iodine lasers, but  $\text{C}_3\text{F}_7\text{I}$  produces the greatest power output. The iso state of  $\text{C}_3\text{F}_7\text{I}$ , in which the iodine atom is attached to the side of the chain, produces slightly more laser output than the normal state. Therefore, this molecule was used in the laser. Some free-iodine atoms combine to form iodine molecules, but most recombine with the  $\text{C}_3\text{F}_7$  free radical to regenerate the lasing gas. These chemical reactions are discussed in detail by Davis et al.<sup>5</sup>

The energy level of the excited iodine atom is split by the interaction of the electron angular momentum of 1/2 with the nuclear angular momentum of 5/2. A diagram of these energy levels is shown in Fig. 2. The F-values are the sums of the electron angular momentum J-value and the nuclear angular momentum, and the g-values are the degeneracy of each state. As a result of the splitting of the energy levels, six spectral lines are allowed by the selection rules. Their relative strengths and shifts are shown in Fig. 2. At a pressure of 15 Torr, the spectral lines are clearly separated. Most of the laser radiation appears in the 3-4 line. The lifetime of the  $^2P_{1/2}$  excited state of iodine is relatively long ( $\sim 0.2$  sec).

Davis et al.<sup>5</sup> noted that the spectral lines could be further split and shifted by the strong magnetic field associated with a high-current

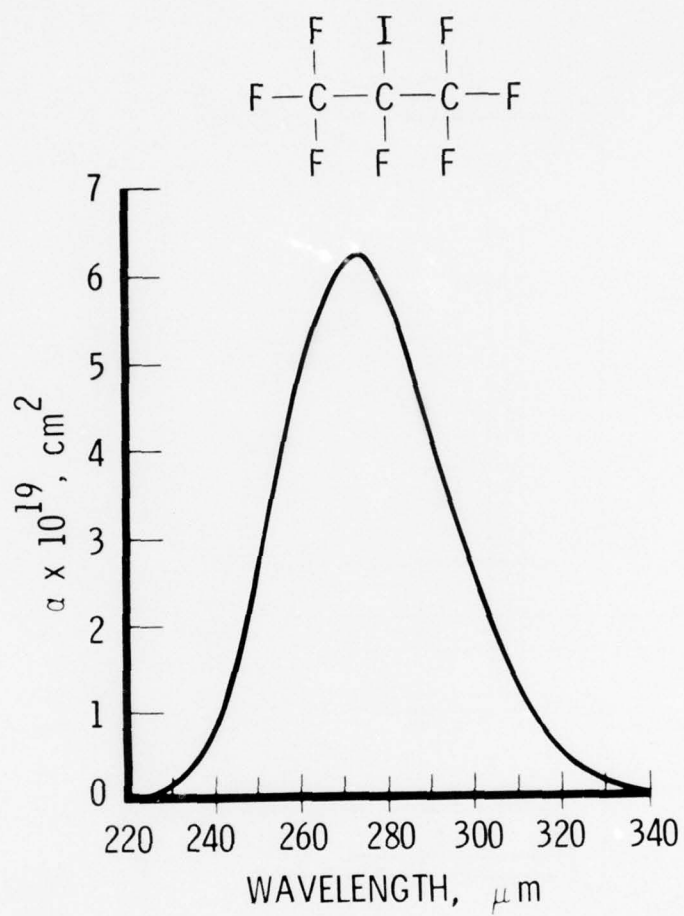


Fig. 1. Ultraviolet Absorption of  $\text{C}_3\text{F}_7\text{I}$



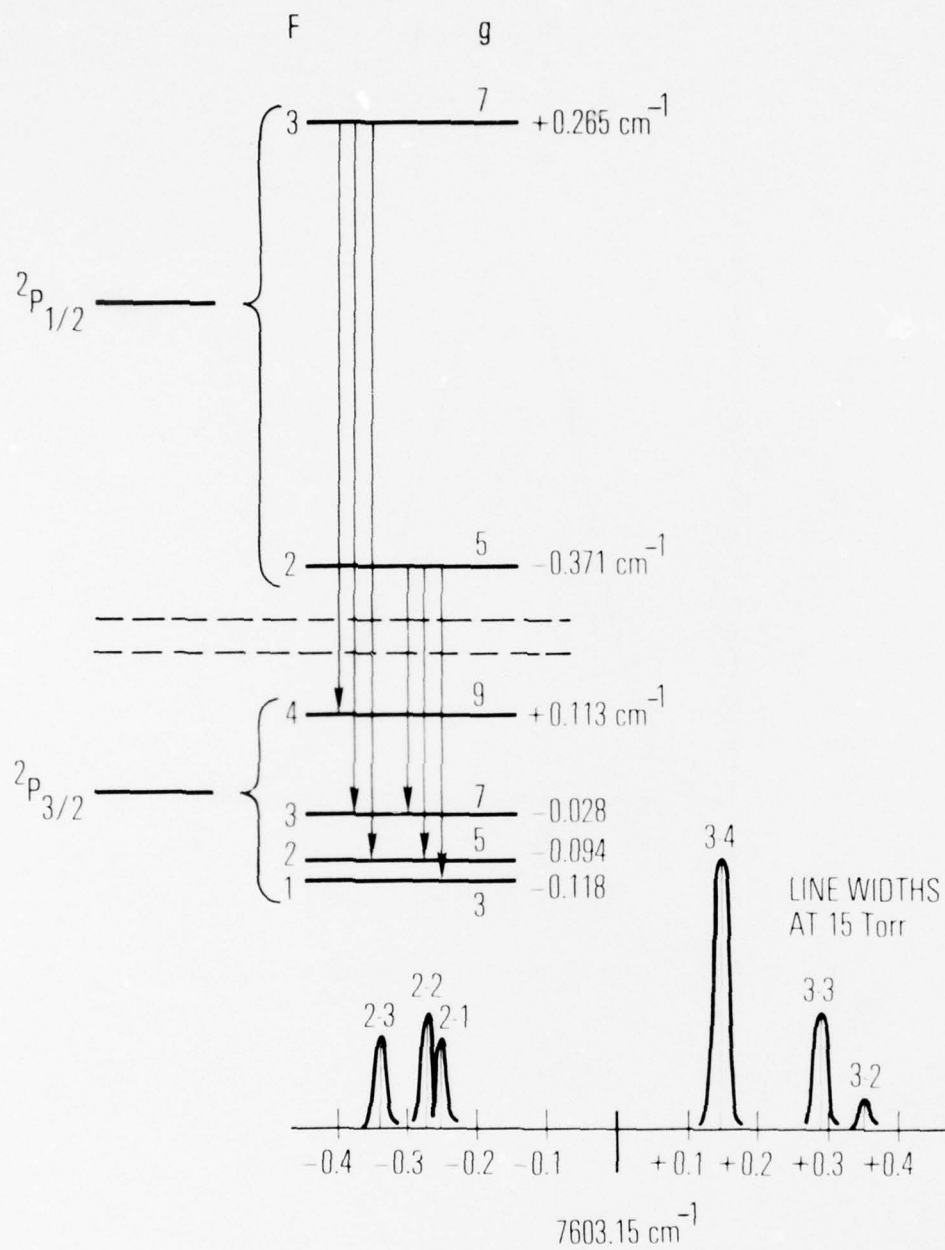


Fig. 2. Energy Levels of Excited and Ground States of Atomic Iodine and Allowed Transitions

flashlamp. In this configuration, however, the magnetic field is mostly confined near the flashlamp tube by close-fitting current return bus rods, and the amount of magnetic field in the laser tube volume is small (Section IV).

### III. PERFORMANCE CALCULATIONS

The operating parameters that produce the desired small signal gain and the corresponding output energy were calculated. These performance calculations were based on the analysis developed by Trenholme and Manes<sup>7</sup> and on data from Hohla and Kompa.<sup>4</sup>

The small signal gain is the product of the cross section for stimulated emission ( $\sigma$ ) and the inversion density ( $\Delta N$ ). The latter is given by

$$\Delta N = 3.5 \times 10^{16} \delta P_{CF}$$

where  $\delta$  is the degree of dissociation, which depends on the integrated ultra-violet radiation from the flashlamp and  $P_{CF}$  is the partial pressure of  $C_3F_7I$  in Torr. The numerical factor of  $3.5 \times 10^{16}$  is, of course, the number of molecules per cubic centimeter at a pressure of 1 Torr. The cross section for stimulated emission ( $\sigma$ ) is inversely proportional to the spectral line width, and the line width is directly proportional to the pressure in the range where pressure broadening is much greater than the Doppler width, i.e., when  $P_{CF} > 10$  Torr. Then,  $\sigma = \sigma_0 / P_{CF}$ . The value of  $\sigma_0$  is  $6 \times 10^{-17} \text{ cm}^2$  per unit of pressure in Torr. From the above, the small-signal gain ( $g_0$ ) is

$$g_0 = 3.5 \times 10^{16} \sigma_0 \delta$$

or

$$g_0 = 2.1 \delta (\text{cm}^{-1})$$

<sup>7</sup> J. B. Trenholme and K. R. Manes, "A Simple Approach to Laser Amplifiers," UCRL-51413, Lawrence Livermore Laboratory, University of California, Livermore, Calif. (28 November 1972).

The iodine spectral lines can be broadened further, and the gain reduced by the addition of diluent gases such as argon or  $\text{CO}_2$ . An estimate of  $\delta$  will be made later in this section.

It is necessary to determine the saturation energy density  $E_s$  in order to calculate the maximum energy density that can be extracted from the medium.

$$E_s = \left(\frac{a}{\gamma}\right) \left(\frac{h\nu}{\sigma}\right) (\text{J/cm}^2)$$

$\gamma$  is a factor that depends on the degeneracies of the upper and lower levels, i.e.,  $\gamma = (1 + g_u/g_l)$ . The  $a$  is the fraction of iodine atoms in the excited level that contribute to lasing. At low pressure, only the 3-4 line lases.  $\gamma = 16/9$  and  $a = 7/12$ ; therefore,  $a/\gamma = 0.33$  (Fig. 2). At higher pressures, the lines overlap, and  $a/\gamma$  can be as great as 0.67.  $h\nu = 1.5 \times 10^{-19}$  J for  $\lambda = 1.315 \mu\text{m}$ , and  $\sigma = 6 \times 10^{-17}/P_{\text{CF}}$ . Thus,

$$E_s = 0.33 \times \frac{1.5 \times 10^{-19}}{6 \times 10^{-17}} P_{\text{CF}} = 8.25 \times 10^{-4} P_{\text{CF}} (\text{J/cm}^2)$$

The maximum extractable energy density ( $E_{\text{EX}}$ ) is equal to  $g_0 E_s (\text{J/cm}^3)$ .

$$E_{\text{EX}} = 8.25 \times 10^{-4} P_{\text{CF}} \times 2.16 = 1.74 \times 10^{-3} P_{\text{CF}} (\text{J/cm}^3)$$

Experience at the Garching laboratory of the Max-Planck-Institute für Plasmaphysik, Garching, Germany, has shown a flashlamp efficiency of  $3.3 \times 10^{-3}$  for low-pressure, single-line operation, i.e.,

$$E_{\text{ex}} V = 3.3 \times 10^{-3} E_{\text{cap}}$$



where  $V$  is the tube volume, and  $E_{\text{cap}}$  is the electrical energy stored in the discharge capacitor. The volume of an annular laser tube is

$$V = \pi L(r_2^2 - r_1^2)$$

where  $L$  is the length, and  $r_2$  and  $r_1$  are the outer and inner diameters, respectively. The above expression can be written

$$V = \pi L(r_2 - r_1)(r_2 + r_1) = \pi Ld(r_2 + r_1)$$

where  $d$  is the thickness of the annular space. Then,

$$E_{\text{ex}} V = 1.74 \times 10^{-3} \delta P_{\text{CF}} \pi Ld(r_2 + r_1)$$

The optimum value of the product of  $P_{\text{CF}}d$  is determined by the absorption coefficient of  $\text{C}_3\text{F}_7\text{I}$ , which is  $\alpha = 1/85 \text{ (Torr cm)}^{-1}$ . For uniform pumping through the thickness ( $d$ ),  $\alpha P_{\text{CF}}d = 1$ ; then,  $P_{\text{CF}}d = 85$ , and

$$E_{\text{ex}} V = 0.462 \delta L(r_2 + r_1) \text{ J} = 3.3 \times 10^{-3} E_{\text{cap}}$$

For this iodine laser tube,  $r_1 = 5.6 \text{ cm}$ ,  $r_2 = 10.0 \text{ cm}$ ,  $L = 100 \text{ cm}$ , and  $E_{\text{cap}} = 5000 \text{ J}$ . With these values used in the equation above,  $\delta$  is 0.023, and  $E_{\text{ex}} V = 16.5 \text{ J}$ . The gain ( $g_0$ ) is  $2.1\delta = 0.0483 \text{ cm}^{-1}$  and  $g_0 L = 4.83$ .

These calculations are approximate and depend on the value of the flashlamp efficiency. Since the flashlamp geometry reported here is different from that used at Garching, this value may be significantly different. The gain ( $g_0$ ) can be increased somewhat by means of a slightly lower pressure than the 19 Torr implied by  $P_{\text{CF}}d = 85$ . The medium uniformity thereby would be improved, but the output energy would be decreased slightly. For

a pressure ( $P_{CF}$ ) of 15 Torr, it was found that  $\delta = 0.0295$  and  $g_0 = 0.062$ . These values come close to satisfying the gain requirements for the iodine laser.

The uniformity of the annular medium was examined. The degree of dissociation is, of course, proportional to the flux from the flashlamp. The flux ( $F$ ), at any given radius ( $r$ ) from the center of the annulus, is given by

$$\frac{F(r)}{F(r_1)} = \frac{r_1}{r} e^{-k(r-r_1)}$$

when the flux escapes through the outer tube. If, however, part of the light is reflected from the outer tube with a reflection coefficient ( $\beta$ ), the pumping radiation is the sum of the outgoing and reflected radiation.

$$\frac{F(r)}{F(r_1)} = \frac{r_1}{r} e^{-k(r-r_1)} + \beta \frac{r_1}{r} e^{-k(r_2-r_1)} e^{-k(r_2-r)}$$

These flux values are plotted in Fig. 3 as a function of radius for both of the above cases and for several values of the absorption parameter ( $k$ ), which is related to the partial pressure of  $C_3F_7I$ . The above relations neglect the loss of absorbing molecules caused by dissociation, so the results are valid for only a small degree of dissociation. There is a radial dependence of  $r_1/r$  for zero absorption. Reflection from the outer tube increases the radiation flux and improves the medium uniformity somewhat. For all experiments, a covering of aluminum foil was placed around the outside tube to reflect the light back into the annular medium.

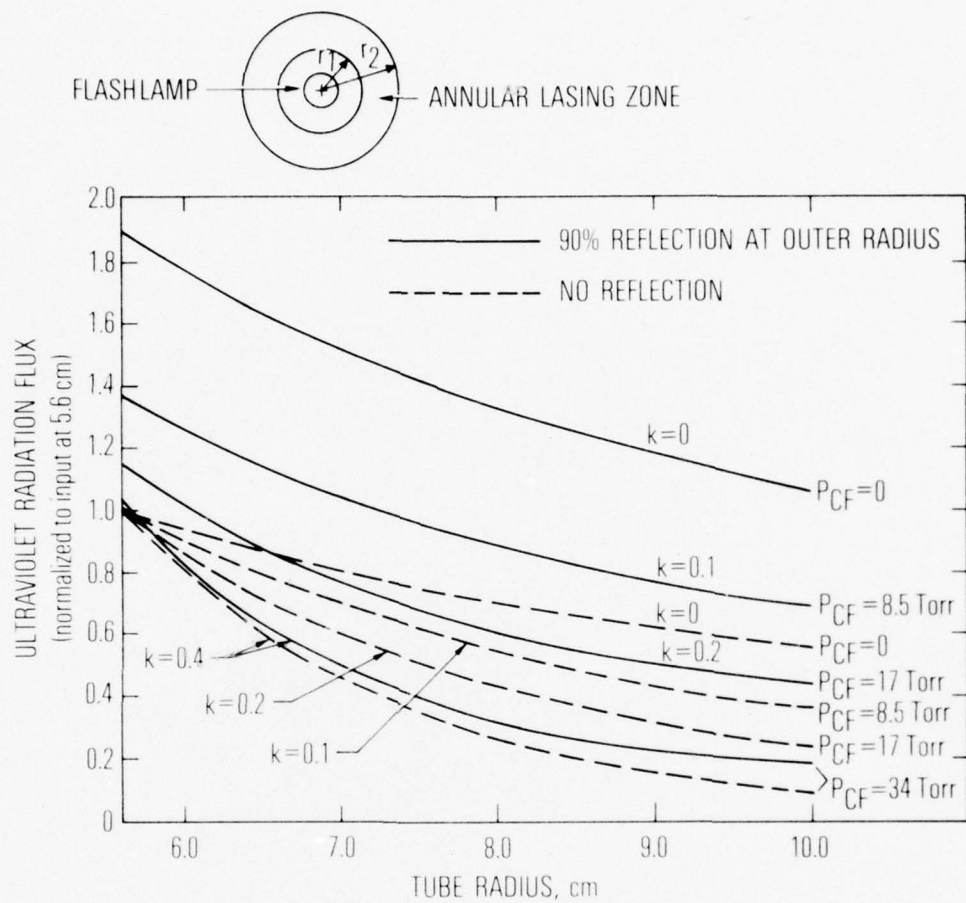


Fig. 3. Distribution of Radiation Flux in Annular Lasing Zone

#### IV. HIGH-VOLTAGE ELECTRICAL CIRCUITS

##### A. SYSTEM DESIGN

Figure 4 is a schematic diagram of the high-voltage electrical circuits. The system is designed to discharge an energy storage capacitor into a flashlamp. It was desired that the duration of the current pulse be minimized. The capacitor is charged with a high-voltage power supply, rated at 70 kV and 5.5 mA, through a 10-M $\Omega$  resistor. All of the high-voltage leads were completely enclosed for personnel safety.

##### B. CHARGING CIRCUIT

The high-voltage power supply is a Universal Voltronics Model BAM-70-5.5 adjustable dc supply with a standard Minitrol control panel. The charging current is limited by a 10-M $\Omega$  resistor, which gives an RC time constant of 26.3 sec. The capacitor voltage is given by the equation

$$V_c = V_o (1 - e^{-t/RC})$$

where  $V_o$  is the supply voltage and  $t$  is the time. The time required to charge a capacitor to a voltage ( $V_c$ ) with a power supply with an output voltage ( $V_o$ ) is then

$$t = RC \ln \left( \frac{V_o}{V_o - V_c} \right)$$

For  $V_o = 70$  kV and  $V_c = 60$  kV, the charging time is 51.6 sec.

A liquid resistor, containing a nearly saturated  $\text{CuSO}_4$  solution, is a simple and inexpensive capacitor dump resistor. This resistor is made of a piece of 1/2-in. i.d. tygon tubing 16 in. long with copper electrodes at the ends. It was calculated that the total energy (4734 J) stored in the 2.63- $\mu\text{F}$



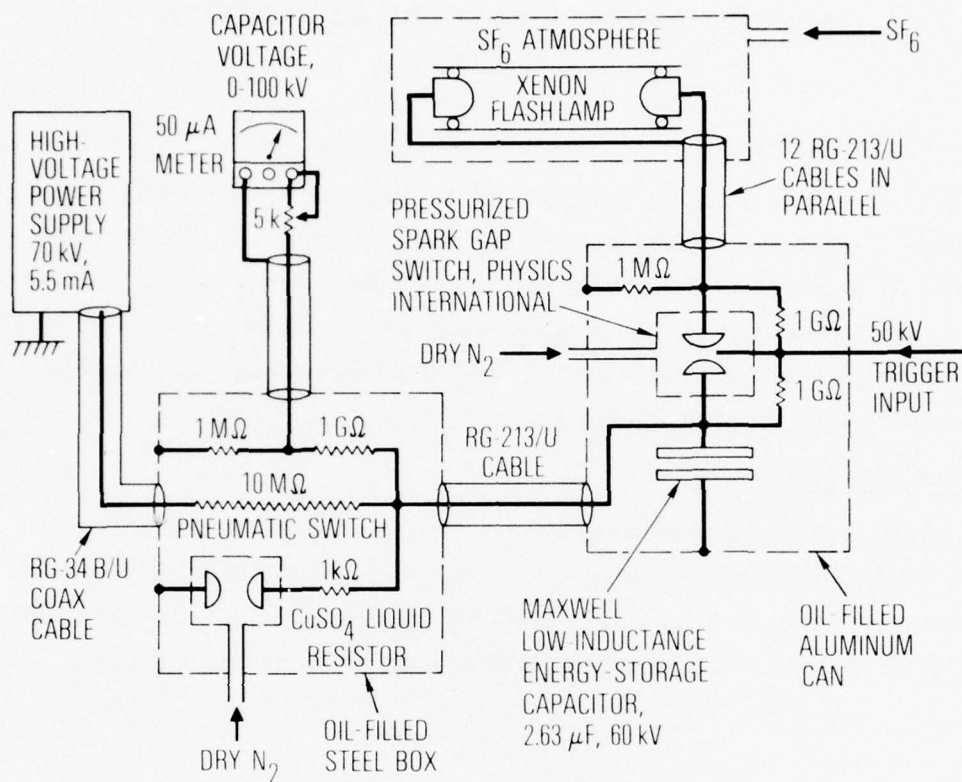


Fig. 4. Schematic Diagram of High-Voltage Circuits

capacitor at 60 kV would cause a 22° C temperature rise in this dump resistor. The measured resistance was 1000  $\Omega$ , so the RC time constant is 2.63 msec, and the peak current is 60 A. The pneumatic switch that closes the circuit through the dump resistor is normally closed with no air pressure. The pneumatic switch is opened by nitrogen pressure when the capacitor is charged, but it can be quickly closed by a fast-acting pressure-relief valve.

The voltage on the capacitor is measured directly with a 50- $\mu$ A meter connected to the capacitor through a 1-G $\Omega$  resistor. This voltage measurement resistor, the charging resistor, the liquid dump resistor, and the pneumatic switch are mounted in a steel box filled with transformer oil. All high-voltage connections are fitted with corona balls.

#### C. CAPACITOR AND SPARK SWITCH

The capacitor is a Maxwell Model 32503 low-inductance, energy storage capacitor designed for nonoscillatory service, i.e., small voltage reversal. The measured capacity is 2.63  $\mu$ F. A Physics International Model 670 high-voltage, high-current, spark-gap switch is mounted on the high-voltage electrode of the capacitor as shown in Fig. 5. Connections are made to the flashlamp with 12 RG-213/U coaxial cables. The spark-gap switch is triggered by a fast-rising, high-voltage pulse from a Tobe Deutschmann pulse generator, which, in turn, requires a fast rising 250-V trigger. The spontaneous breakdown potential (of the spark-gap switch) is made somewhat higher than the operating voltage by adjusting the gas pressure in the switch. For 60 kV, a pressure of about 50 psig of nitrogen is required, but atmospheric pressure of SF<sub>6</sub> is more than adequate. The SF<sub>6</sub> gas is preferred because the switch becomes erratic after many firings with nitrogen gas.

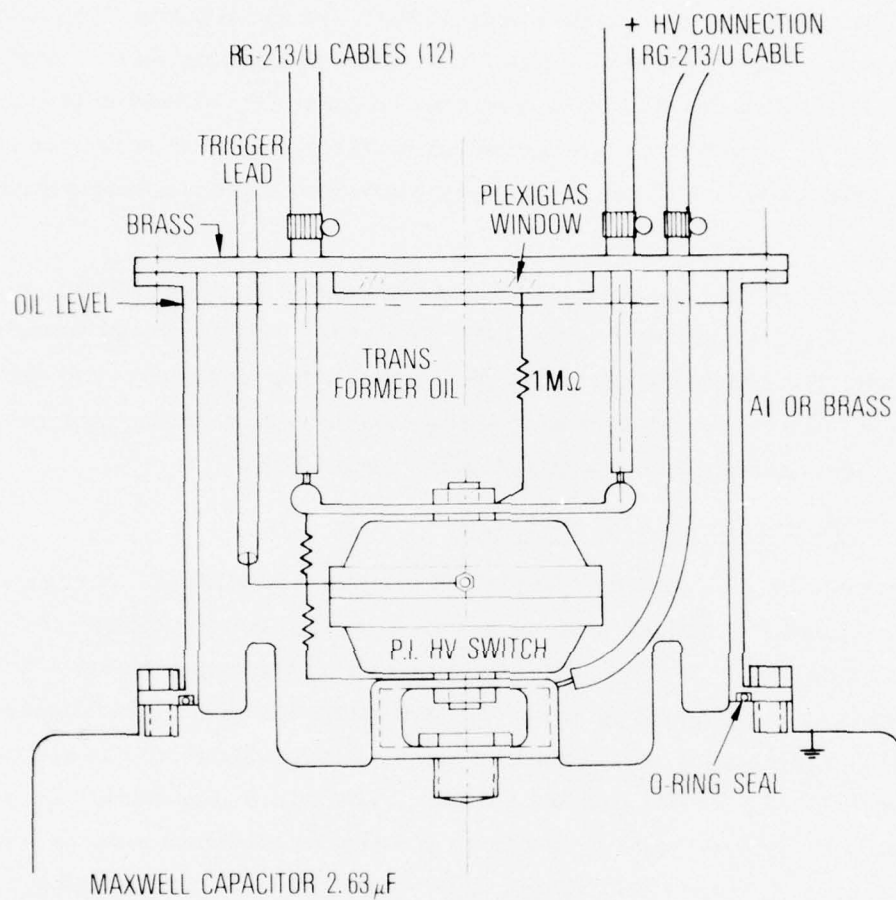


Fig. 5. High-Voltage Switch

#### D. FLASHLAMP

A paper by Holzrichter and Schalow and<sup>8</sup> design information from the group at Garching<sup>\*</sup> were very helpful in the design of the flashlamp. The requirements on the flashlamp were to radiate a 1-m length of lasing medium with ultraviolet radiation in the region of 2700 Å. On the basis of Garching experience,<sup>\*</sup> a relatively large internal diameter of 18 mm was chosen to increase the opacity of the ultraviolet radiation. It was planned to use a single capacitor of about 5000-J energy storage capacity. Commercial-quality fused quartz was used for the flashlamp, which begins to absorb at wavelengths below 2600 Å, but this absorption was not large enough to significantly degrade the output.

From the analysis by Holzrichter and Schalow,<sup>8</sup> a parameter ( $K_o$ ) was calculated from the relation  $K_o = k\ell/d$ , where  $\ell$  is the distance between the electrodes,  $d$  is the tube diameter, and  $k$  is a constant equal to 1.2. The voltage across the flashlamp is assumed to be proportional to the square root of the current

$$V = K_o \sqrt{i}$$

A characteristic impedance ( $Z_o$ ) is given by  $Z_o = \sqrt{L/C}$ . For a circuit inductance of 0.25  $\mu$ H and a capacitance of 2.63  $\mu$ F,  $Z_o$  is 0.3083  $\Omega$ . A characteristic time constant ( $T$ ) is given by  $T = \sqrt{LC}$ . For these values of  $L$  and  $C$ ,  $T$  is 0.811  $\mu$ sec. A damping constant ( $\alpha$ ), is defined by  $\alpha = K_o/\sqrt{Z_o V_o}$ . For  $V_o = 50$  kV,  $\alpha$  is 0.537, and, for  $V_o = 60$  kV, 0.490. From the parametric curves of normalized current versus normalized time given by Holzrichter and Schalow for  $\alpha = 0.5$ , the peak current was found to be  $0.65 V_o/Z_o$ . For

---

<sup>\*</sup>R. F. W. Gross, The Aerospace Corporation, unpublished.

<sup>8</sup>J. F. Holzrichter and A. L. Schalow, "Design and Analysis of Flashlamp Systems for Pumping Organic Dye Lasers," Ann. N. Y. Acad. Sci. 168, 703 (1970).

$V_o = 60\text{kV}$ ,  $I_p = 126,500\text{ A}$ , and, for  $V_o = 50\text{ kV}$ ,  $I_p = 102,000\text{ A}$ . From the parametric curves of current versus time, it was found that the half period of the current pulse for  $\alpha = 0.5$  is  $3.25\text{ T}$ , which is  $2.64\text{ }\mu\text{sec}$ . The theoretical current pulse for  $V_o = 50\text{ kV}$  is shown in Fig. 6, and an actual current trace is shown in Fig. 11.

Figure 7 is a simplified cross-sectional drawing of the laser device. The 12 coaxial cables from the spark-gap switch are attached radially to a cylindrical electrode housing. The outside shields of the coaxial cables, which are grounded, are attached to the outer shell of the housing, and the central conductors of the coaxial cables are connected to the high-voltage electrode. The ground electrode of the flashlamp is connected to the electrode housing by three small cylindrical rods around the flashlamp. The magnetic field associated with the flashlamp current is mostly confined between the flashlamp and the ground return rods, so that the energy levels of the excited iodine atoms in the annular region are affected very little by Zeeman splitting.

A formula that appears to describe the functional behavior of the flashlamp's explosion limit was given by Holzrichter and Schlow<sup>8</sup>

$$E_x = b \ell d \sqrt{T}$$

where  $b$  is a constant about  $6.8 \times 10^4\text{ J cm}^2\text{ sec}^{1/2}$ . For the parameters of this study,  $E_x = 11,000\text{ J}$ . The lamp therefore is operated well below the explosion limit.

A potential problem that had to be addressed in this design of the flashlamp circuit in which the ground return rods were used was the electromagnetic forces on these rods. The magnetic field associated with the flashlamp current is  $B_\theta = \mu_o I / 2\pi R$ . For  $I = 120,000\text{ A}$ , the value of  $B_\theta$  at the rod position of  $R = 1.9\text{ cm}$  is  $B_\theta = 1.26\text{ Wb/m}^2$ . Each rod carries a



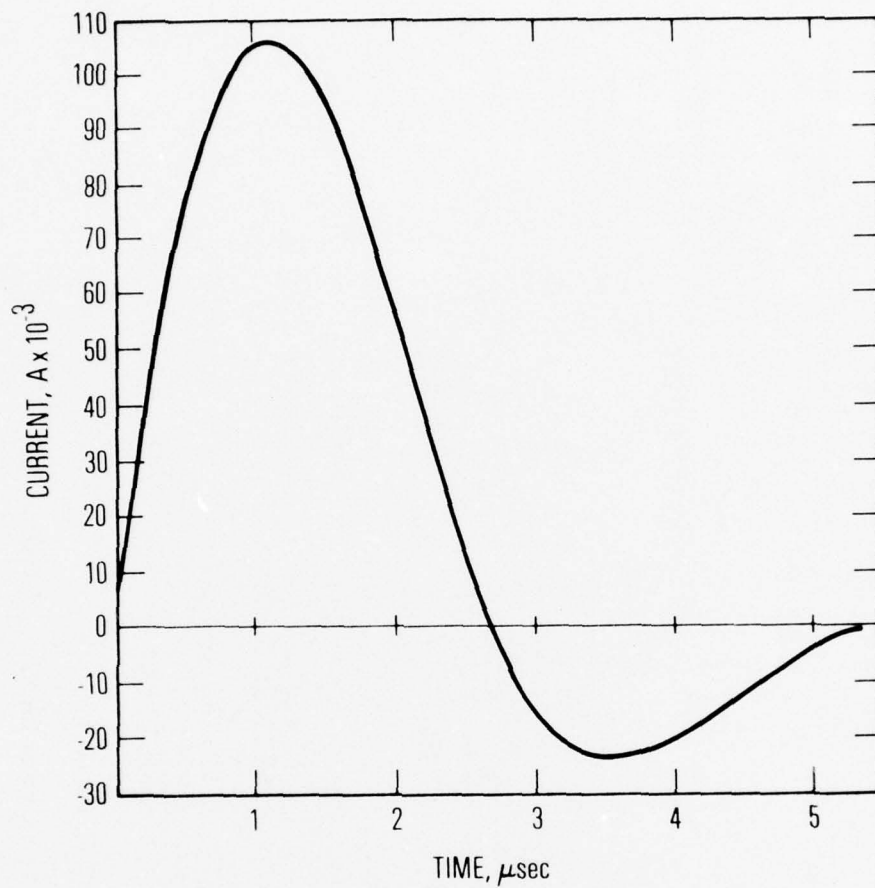


Fig. 6. Theoretical Flashlamp Current Pulse for  $V_c = 50 \text{ kV}$

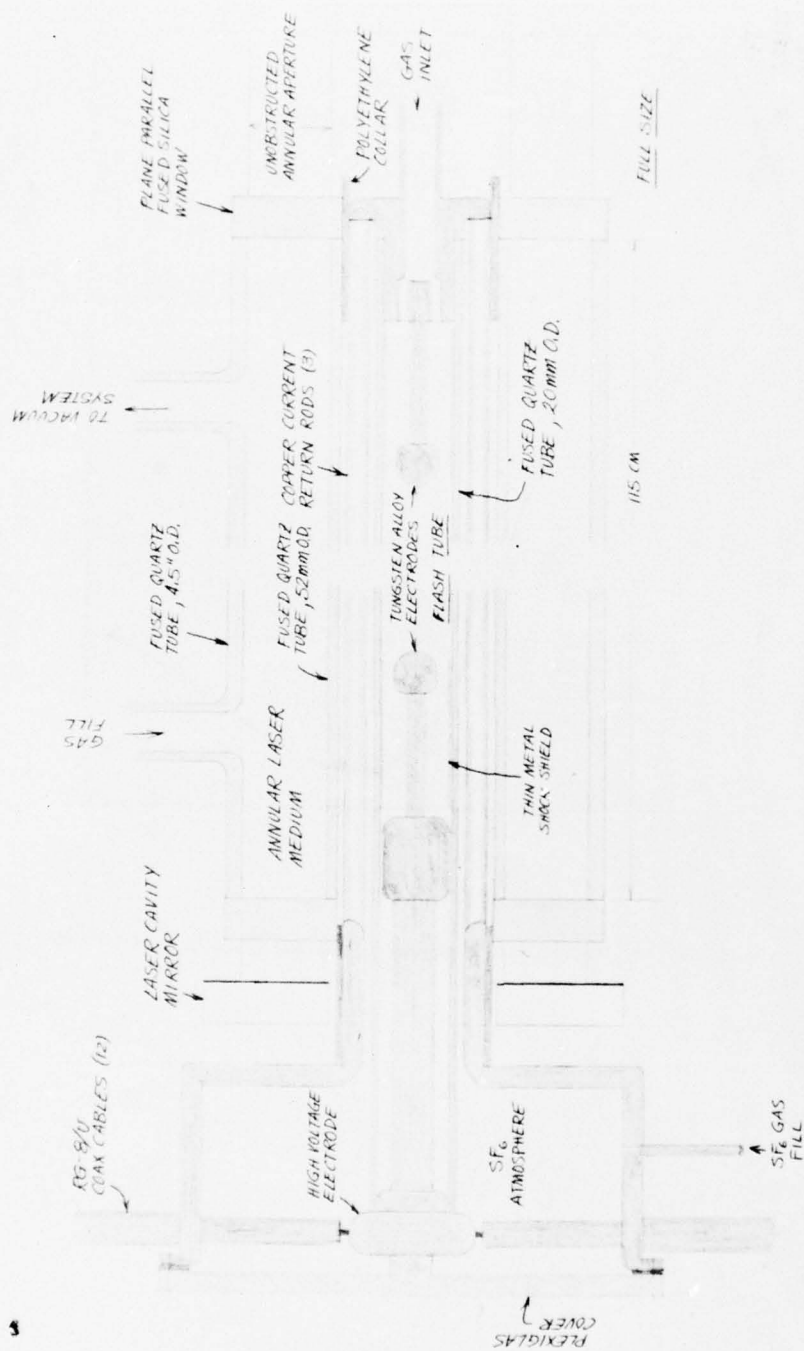


Fig. 7. Cross Section of Iodine Laser

maximum current of 40,000 A; therefore, the  $J \times B$  force per rod is  $1.26 \times 40,000 = 50,400$  N/m. A constant force of this magnitude would tear the rods apart, but the duration of the force is short ( $\sim 2 \mu\text{sec}$ ). The rods, therefore, receive an impulse of 0.1 N-sec/m, which can then be absorbed by restraining supports over a much longer period of time. The forces on the support structure are then greatly reduced. A detailed design calculation of the response and the required strength of the restraining support rings was considered too complicated, so a conservative estimate was made that the forces on the support structure were reduced by a factor of 100. A design based on this estimate proved to be satisfactory. Brass support rings 1/8-in. wide and 1/16-in. thick were welded every 6 in. along the length of the rods.

High-voltage insulation was a critical problem, especially with the close-fitting ground return rods and housing. A flashlamp wall thickness of 3 mm was required to provide a dielectric strength of 60 kV between the high-voltage electrode and the ground return rods and electrode housing. The electrode spacing in the housing was inadequate to prevent voltage breakdown in air; therefore, an atmosphere of  $\text{SF}_6$  was necessary. Silicone rubber seals were used between the inner laser tube and the electrode housing and the ground electrode to contain the  $\text{SF}_6$  gas. The  $\text{SF}_6$  gas was fed slowly into the electrode housing and then flowed out through a small hole in the seal around the ground electrode. This scheme worked well, and the only electrical breakdowns occurred when the  $\text{SF}_6$  was not flowing in the electrode housing. The  $\text{SF}_6$  gas does not absorb the ultraviolet radiation used to pump the iodine laser. All electrical connections were silver-soldered or clamped very tightly to avoid contact arcing caused by the high peak current.

### E. INDUCTANCE CALCULATIONS

The total inductance of the flashlamp circuit was previously stated to be 0.025  $\mu$ H. A summary of the calculations for the inductance is given in this section.

A useful formula for the inductance of coaxial cables is  $L = 2l$  (cm)  $\ln$  (b/a) nanoH. For the RG-8/U coaxial cable,  $L = 2.75$  nanoH/cm. For 12 cables in parallel,  $L = 22.9$  nanoH/m, and for the 2-m length actually used,  $L = 45.8$  nanoH.

The calculation of the inductance for the flashlamp with the ground return rods and electrode housing is more complex. The inductance of the flashlamp is calculated with one rod and then divide by three. The formula used is

$$L = 2 \ln d^2 / \rho_1 \rho_2 \text{ nanoH/cm.}$$

where  $\rho_1$  and  $\rho_2$  are the diameters of the flashlamp and rod conductors, respectively, and  $d$  is the spacing between centers of the conductors.

$$L = 2 \ln \frac{1.85^2}{1.6 \times 0.625} = 2.46 \text{ nanoH/cm}$$

For three return rods 117 cm long,  $L_1 = 177 \times 2.46/3 = 96$  nanoH. There is a short length, 5 cm, of a close-fitting coaxial ground electrode of 3.2 cm diameter. The high-voltage electrode has a diameter of 1.2 cm in this region. Therefore,

$$L_2 = 2 \times 5 \ln \left( \frac{3.2}{1.2} \right) = 9.8 \text{ nanoH}$$

---

<sup>9</sup>F. W. Grover, Inductance Calculations, Working Formulas and Tables, Dover Publications, New York (1962).

The cylindrical housing is 4.5-cm long and has a diameter of 12.8 cm. Thus,  $L_3 = 2 \times 4.5 \ln(12.8/1.2) = 21.3$  nanoH. The total inductance of the flashlamp and electrode connections is  $L = L_1 + L_2 + L_3 = 127.1$  nanoH.

The inductance contributions of the individual elements are:  $L_{\text{capacitor}} = 15$  nanoH,  $L_{\text{cables}} = 45.8$  nanoH,  $L_{\text{lamp}} = 127.1$  nanoH, and  $L_{\text{switch}} = 60$  nanoH. The last figure is an estimate. The total circuit inductance is the sum of the above, i.e.,  $L_{\text{total}} = 250$  nanoH.



## V. LASER-TUBE FABRICATION

The tube was fabricated from commercial fused-quartz tubing with optical-quality, fused-silica end windows. The windows were fabricated from Dynasil Type 4102 fused-silica disks 5/8 in. thick. They were optically ground and polished flat on both sides to about  $\lambda/10$  (visible) and then coated with antireflection layers (at = 1.3  $\mu\text{m}$ ).

The outside of the inner annular tube was sandblasted, and the inside of the outer tube was ground to eliminate specular reflections from the surface that might cause parasitic stimulated emission. The grinding of the outer tube was accomplished by rotating the tube for several hours with a mixture of coarse alumina grinding powder and porcelain balls. The ends of the cylindrical tubes had to be cut accurately to cement the end windows with minimum gaps. Also, the ends were cut at a small angle to one another to prevent multiple reflections between the end windows. The inner and outer tubes were held in precise alignment with each other during cutting with a diamond saw by waxing the tubes together with hard optical wax.

Torr Seal epoxy cement supplied by Varian Associates Vacuum Division was used for cementing the end windows to the annular tubes. It was necessary to make end jigs to hold the parts in alignment while tacking the pieces together. The joints were then carefully cemented for a vacuum tight seal.

## VI. VACUUM AND GAS-HANDLING SYSTEM

The vacuum and gas-handling system is shown schematically in Fig. 8. A small oil diffusion pump is used to pump out the system to a vacuum of less than  $10^{-4}$  Torr. A flexible metal bellows tube connects the manifold to the laser tube. The vacuum manifold is also used to pump out and fill the xenon flashlamp. Pressures are measured by a Bourdon tube gauge. The xenon flashtube, for example, is filled with about 50 Torr of xenon and is then disconnected from the system. This fill is good for at least 50 shots. The  $C_3F_7I$  is stored in a pyrex flask that can be cooled with liquid nitrogen. The usual procedure for filling the laser tube is to allow the  $C_3F_7I$  to warm up slowly from liquid nitrogen temperature with the valve to the flask opened. The vapor pressure increases with temperature (Fig. 9), and the valve to the flask is closed when the desired pressure ( $\sim 20$  Torr) is reached. A single fill of  $C_3F_7I$  can be used for up to 20 shots with only slight deterioration in output energy. The gas finally becomes contaminated with iodine, which quenches the excited iodine atoms, and other products of the flash photolysis. This material can be pumped out into a waste cylinder cooled to liquid nitrogen temperature. Iodine was observed to condense on the walls but disappeared after pumping overnight.

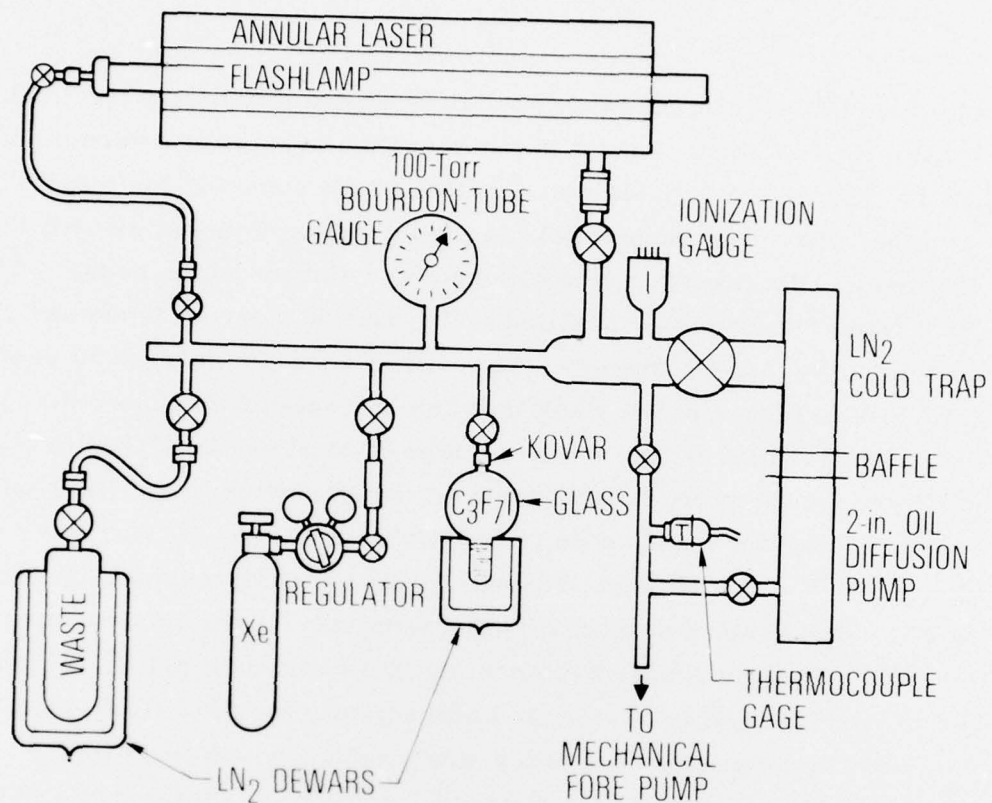


Fig. 8. Schematic Diagram of Vacuum and Gas-Handling System

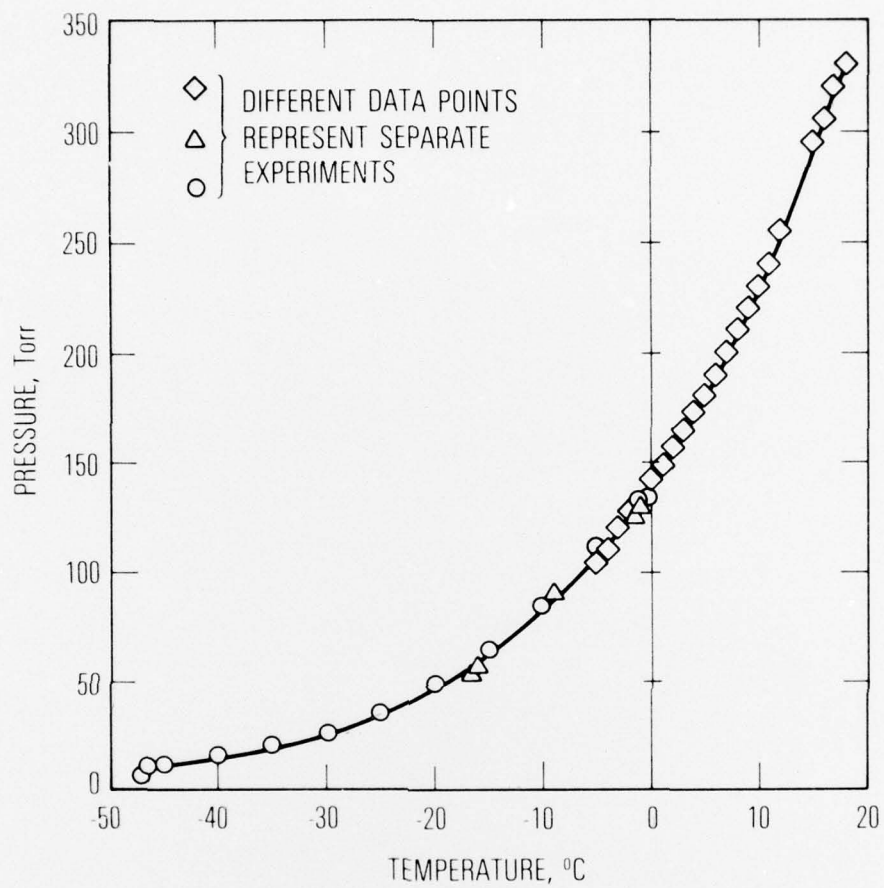


Fig. 9.  $C_3F_7I$  Vapor Pressure Versus Temperature  
(From J. G. Coffey, The Aerospace Corporation)



## VII. PERFORMANCE

The iodine laser was first tested with a Fabry-Perot resonator consisting of a fully reflecting mirror and a partially reflecting mirror. Two partially reflecting, plane, parallel plates were fabricated from optical-quality fused silica. They were coated with an antireflective coating on one side and with a nonabsorbing, partially reflecting coating on the other side, with reflectivity values of 80 and 50%, respectively. The partially reflecting plate of the Fabry-Perot resonator was aligned parallel with the flat mirror by means of a small He:Ne laser beam.

The intensity distribution of the near field was recorded with an infrared vidicon camera with an RCA Iricon tube. The laser beam obtained with the Fabry-Perot resonator illuminated a sand-blasted, black-anodized aluminum screen that was focused onto the infrared vidicon. The vidicon image was recorded and then displayed on a monitor, which was photographed with a Polaroid oscilloscope camera. Figure 10 is a typical photograph of the near-field intensity distribution. A radial decrease in intensity is evident, as expected, and the three current return rods create distinct shadows in the output distribution.

The flashlamp current was sensed with a small probe coil mounted inside the electrode housing near the wall. This signal is proportional to  $dB/dt$ ; the signal was integrated with an RC circuit to obtain a voltage proportional to the current. From the geometry, it was calculated that  $I = 6 \times 10^5 V_{out}$ . The detailed calculations are given in Appendix B. An intrinsic germanium detector, operated at room temperature, was set up to monitor the laser radiation. The detector response extends to  $1.8 \mu m$ , and, therefore, it is sensitive at the iodine-laser wavelength of  $1.315 \mu m$ . The detector is normally used in the photovoltaic mode, but it was converted for use in the photoconductive mode by a  $-6V$  bias. A relatively low load resistance of  $100 \Omega$  was used. The detector should therefore be linear at signal levels of



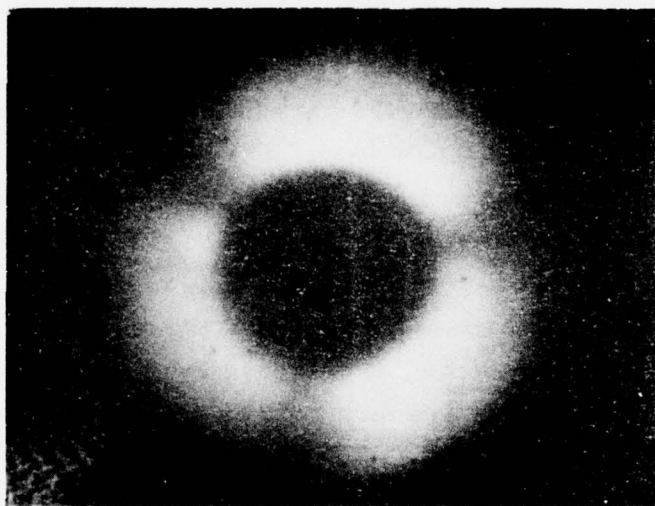


Fig. 10. Near-Field Intensity Distribution  
of Iodine Laser with Fabry-  
Perot Resonator

several volts—far above the signal levels of  $\sim 100$  mV that were normally used.

For most shots, dual scope traces were made of the current and the laser output. A typical dual scope trace is shown in Fig. 11. The signals are smeared by rf interference (probably from the spark gap trigger) at the beginning of the trace, which makes it difficult to establish zero time. It appears, however, that the current pulse duration (time-to-zero current) is approximately  $4.5 \mu\text{sec}$ . The peak current, for this shot at 50 kV, is approximately 75 kA. Therefore, the pulse duration is longer, and the peak current is less than calculated. The calculated values for 50 kV were 102 kA and  $2.7 \mu\text{sec}$ , respectively. The laser output begins at the time of the peak current and the main pulse lasts for about  $2.5 \mu\text{sec}$  with a lower intensity tail extending beyond.

Focused burn patterns and energy measurements were obtained with the Fabry-Perot resonator with both the 80 and 50% reflecting plates. The output laser radiation was focused with an optical-quality, fused-silica lens of 2.2 m focal length. The resulting spot size of approximately 1 cm diam was indicative of the multimode output from the Fabry-Perot resonator.

The laser pulse energy obtained with the Fabry-Perot resonator was measured with a calorimeter-type laser energy meter. At 60 kV and 20 Torr of  $\text{C}_3\text{F}_7\text{I}$ , the maximum pulse energy was 7.5 J, with the 80% plate. With a 50% plate, however, the maximum pulse energy increased to 12.5 J. This compares favorably with the calculated value of 16.5 J for the total available laser pulse energy. It must be presumed that the resonator is not 100% efficient in extracting the total available energy. Since this comparison with the theoretical performance is quite close, other estimates, such as the degree of dissociation and the gain, are probably also close.

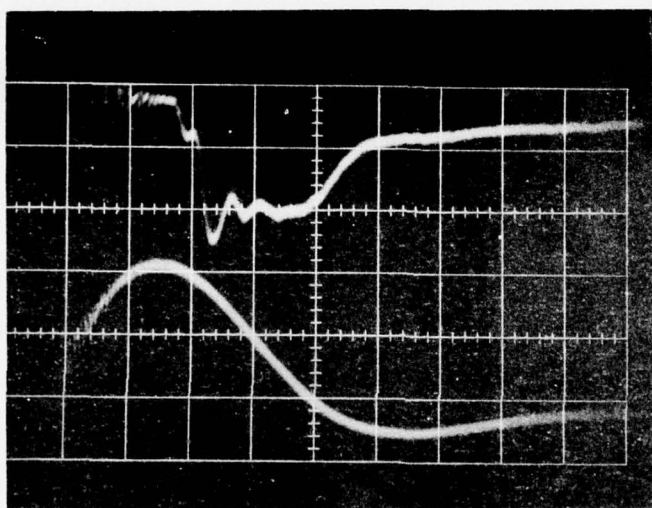


Fig. 11. Oscilloscope Traces of Laser Output and Flashlamp Current. (Sweep speed is  $1 \mu\text{sec/cm.}$ )

## VIII. SUMMARY

The design and performance of an annular iodine laser designed to study annular resonators at a high Fresnel number has been described. The laser medium is pumped by flash photolysis with a high-intensity flashlamp on the axis of the tube. The laser medium is completely unobstructed and accessible to a variety of laser resonators. The laser device was designed to accept a fully reflecting mirror, which covers the entire annular region at the high-voltage end. The medium should be quite homogeneous so that the performance will not be degraded by the gain medium itself.

The laser design appears to fulfill all the requirements, and the performance is close to the theoretical estimates. This laser device, therefore, should provide an excellent facility for testing annular laser resonators at high Fresnel numbers. However, because the laser is a pulsed device, adjustments to resonator elements cannot be made in real time. It is necessary therefore that the alignment of the resonator be accomplished with sufficient precision by means of external alignment devices and that the stability of the resonator base and optical elements be adequate to preserve the alignment.



## APPENDIX A

### THRESHOLD GAIN OF CONVERGING-WAVE, UNSTABLE-CAVITY RESONATOR

The annular iodine laser was initially designed to operate with a converging-wave, unstable-cavity resonator.<sup>1</sup> It was necessary to calculate the threshold gain of this resonator in order to specify the required gain of the iodine laser. Figure A-1 is an optical schematic diagram of the proposed resonator configuration with the annular iodine laser. The resonator was specified as follows:  $R_1 = 150\text{cm}$ ,  $R_2 = -50\text{ cm}$ ,  $\ell = 100\text{ cm}$ , and  $L = 50\text{ cm}$ . In the absence of the double-sided coupling mirror, the round trip magnification (M) of confocal unstable resonator is

$$M = - \left( \frac{R_1}{R_2} \right)$$

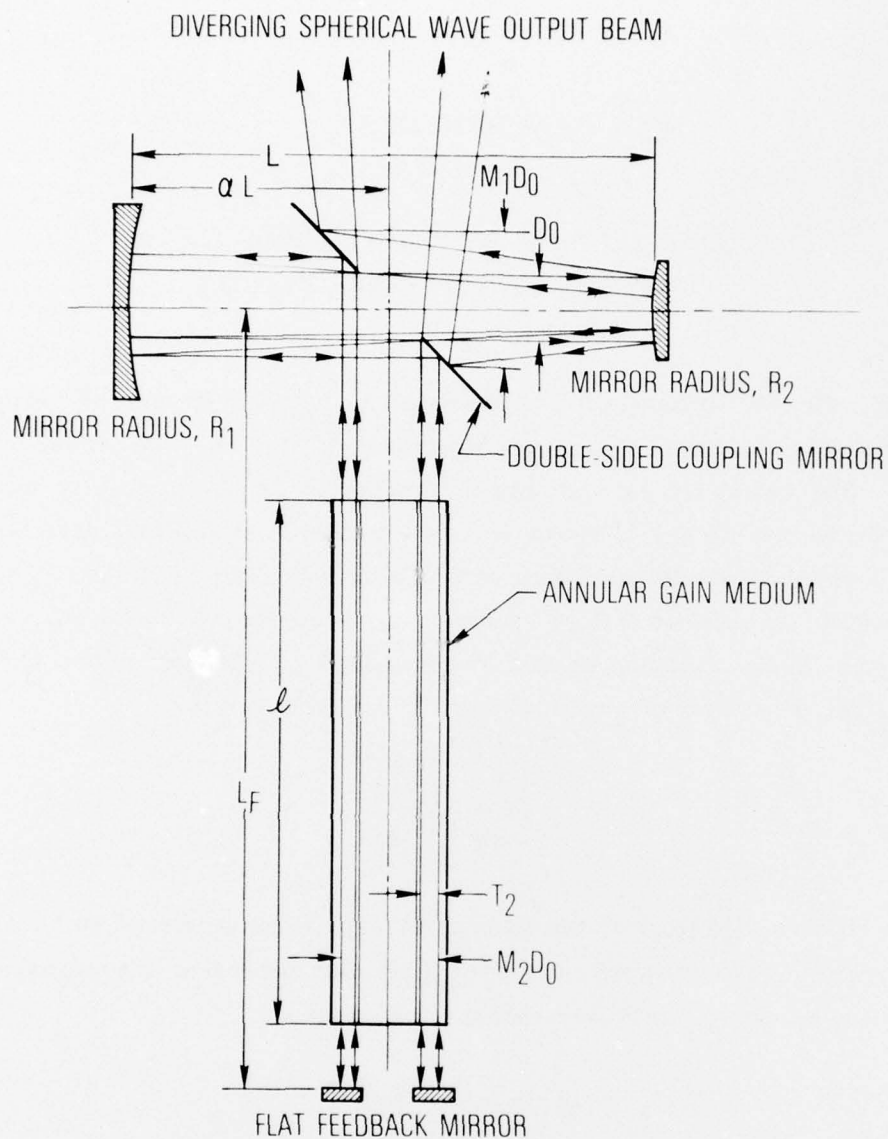
Note that the radius ( $R_2$ ) of the convex mirror is considered to be negative by convention. The magnification ( $M_1$ ) for the diverging wave portion of the converging-wave, unstable-cavity resonator is

$$M_1 = M - \alpha(M - 1)$$

and the magnification ( $M_2$ ) for the parallel beam side can be determined from the relation

$$M_1 M_2 = M$$





NOTE: DIAGRAM IS NOT TO SCALE.

Fig. A-1. Converging-Wave Cavity Schematic Optical Diagram

Chodzko<sup>1</sup> derived the relation for the total reflectivity (r) of the parallel beam of the resonator

$$r = \frac{(1 - 1/M_2^2)}{(1 - 1/M_1^2)}$$

The calculated values of  $M_1$ ,  $M_2$ , and r for a range of values of  $\alpha$  that might be used are given in Table A-1.

Table A-1. Calculated Values of Reflectivity and Theshold Gain

$\alpha$	$M_1$	$M_2$	r	$g_T$
0.25	2.50	1.20	0.34375	0.006455/cm
0.50	2.00	1.50	0.6250	0.003466/cm
0.75	1.50	2.00	0.84375	0.001965/cm

For the calculation of threshold gain, the effective reflectivity ( $r_e$ ) must be used. It is the product of r above and the actual surface reflectivity plus window absorption, and  $r_e = rr_m$ . It is assumed that  $r_m = 0.80$ . The threshold gain per unit length is

$$g_t = \frac{1}{2l} \ln\left(\frac{1}{r_e}\right)$$

## APPENDIX B

### CURRENT MEASUREMENT PROBE

Measurement of the flashlamp current was accomplished with a small current probe located inside the electrode housing near the corner. The signal from the current probe is proportional to  $dB_o/dt$  and thus to  $dI/dt$ ; therefore, the signal must be integrated to display the current pulse on an oscilloscope.

The current probe was made by winding four turns of fine Formvar insulated wire on a No. 10-24 nylon screw. The twisted leads were then connected to a Microdot coaxial-cable connector mounted through the housing. A requirement that the probe coil signal be proportional to  $dB/dt$  is that  $\omega L \ll Z_o$ , where  $Z_o$  is the impedance of the coaxial cable that carries the signal to the oscilloscope. It was calculated that the inductance of the probe coil was  $0.042 \mu H$ ; therefore,  $\omega_o = Z_o/L = 54/0.042 \times 10^{-6} = 1/286 \times 10^9$ , and  $\nu_o = \omega_o/2\pi = 2 \times 10^8$  Hz. Since the Tektronix Type 551 oscilloscope has a bandwidth of only 30 MHz, the requirement that  $\omega L \ll Z_o$  is fulfilled.

The probe coil is located approximately 6 cm from the flashlamp axis. The magnetic field is

$$B = \frac{\mu_o I}{2\pi R} = \frac{4\pi \times 10^{-7}}{2\pi \times 0.06} I = 3.3333 \times 10^{-6} I (\text{Wb/m}^2)$$

The output of the probe coil is  $V_1 = NA dB/dt$ , where  $N$  is the number of turns, and  $A$  is the cross-sectional area of the coil.  $NA = 16\pi \times 10^{-6} \text{ m}^2$ ; thus,  $V_1 = 1.675 \times 10^{-10} dI/dt$ . The integrating circuit consists of a 10-k $\Omega$  resistor and a 0.01- $\mu F$  capacitor, giving a time constant of 100  $\mu\text{sec}$ , which is more than adequate for these measurements. The signal output from the integrator is

$$V_2 = \frac{1}{RC} \int V_1 dt = 1.675 \times 10^{-6} I$$

or

$$I = 6 \times 10^5 V_2$$

The probe coil was not calibrated to verify the calculated constant of proportionality, but the above relation should be fairly close.



#### THE IVAN A. GETTING LABORATORIES

The Laboratory Operations of The Aerospace Corporation is conducting experimental and theoretical investigations necessary for the evaluation and application of scientific advances to new military concepts and systems. Versatility and flexibility have been developed to a high degree by the laboratory personnel in dealing with the many problems encountered in the nation's rapidly developing space and missile systems. Expertise in the latest scientific developments is vital to the accomplishment of tasks related to these problems. The laboratories that contribute to this research are:

Aerophysics Laboratory: Launch and reentry aerodynamics, heat transfer, reentry physics, chemical kinetics, structural mechanics, flight dynamics, atmospheric pollution, and high-power gas lasers.

Chemistry and Physics Laboratory: Atmospheric reactions and atmospheric optics, chemical reactions in polluted atmospheres, chemical reactions of excited species in rocket plumes, chemical thermodynamics, plasma and laser-induced reactions, laser chemistry, propulsion chemistry, space vacuum and radiation effects on materials, lubrication and surface phenomena, photo-sensitive materials and sensors, high precision laser ranging, and the application of physics and chemistry to problems of law enforcement and biomedicine.

Electronics Research Laboratory: Electromagnetic theory, devices, and propagation phenomena, including plasma electromagnetics; quantum electronics, lasers, and electro-optics; communication sciences, applied electronics, semiconducting, superconducting, and crystal device physics, optical and acoustical imaging; atmospheric pollution; millimeter wave and far-infrared technology.

Materials Sciences Laboratory: Development of new materials; metal matrix composites and new forms of carbon; test and evaluation of graphite and ceramics in reentry; spacecraft materials and electronic components in nuclear weapons environment; application of fracture mechanics to stress corrosion and fatigue-induced fractures in structural metals.

Space Sciences Laboratory: Atmospheric and ionospheric physics, radiation from the atmosphere, density and composition of the atmosphere, aurorae and airglow; magnetospheric physics, cosmic rays, generation and propagation of plasma waves in the magnetosphere; solar physics, studies of solar magnetic fields; space astronomy, x-ray astronomy; the effects of nuclear explosions, magnetic storms, and solar activity on the earth's atmosphere, ionosphere, and magnetosphere; the effects of optical, electromagnetic, and particulate radiations in space on space systems.

THE AEROSPACE CORPORATION  
El Segundo, California